J. Opt. A: Pure Appl. Opt. **1** (1999) 185–191. Printed in the UK PII: S1464-4258(99)95742-2

The multiple-mirror lidar '9-eyes'

F Congeduti†, F Marenco†§, P Baldetti‡ and E Vincenti†‖

† Istituto di Fisica dell'Atmosfera (IFA-CNR), Via del Fosso del Cavaliere, 00133 Rome, Italy
‡ Istituto di Fisica dello Spazio Interplanetario (IFSI-CNR), Via del Fosso del Cavaliere, 00133 Rome, Italy

Received 3 July 1998, in final form 17 November 1998

Abstract. The Institute of Atmospheric Physics is developing a large lidar system for atmospheric remote sensing. It will be installed in two containers, to facilitate its deployment at different locations for measurement runs. The emitted wavelengths are 532 and 355 nm, and are obtained with a Nd:YAG laser. The receiver includes three light collectors to split the large dynamic range of the signal incident on each photodetector. The major receiver, to be used for the observation of the middle atmosphere, is an array of nine 0.5 m diameter telescopes (hence the name '9-eyes'). The advantage of the multiple-mirror technique, with respect to a single-mirror receiver, is mainly in the reduced volume, for the same receiving surface (and hence lower cost and transportability). Moreover, the system architecture allows for flexibility in the use of different observation geometries. The other two light collectors are smaller single telescopes, and will be used for the observation of the lower layers of the atmosphere (troposphere and lower stratosphere). Vertical profiles extending from the boundary layer to the mesopause are expected from this instrument, corresponding to a luminous signal spanning over 13 orders of magnitude. Detection of elastic backscattering yields the aerosol profile and information on clouds (base height, optical and geometrical depth of thin clouds). It also provides the molecular density and temperature above ~ 30 km. In the final configuration, the system will also be equipped for the detection of the Raman-scattered signal from N_2 and H_2O, to supply the corresponding vertical distributions.

Keywords: Lidar, remote sensing, optical systems design, telescope, atmospheric temperature structure, atmospheric composition

1. Introduction

The lidar technique for remote sensing of the atmosphere was first used by Fiocco and Smullin (1963) and Ligda (1963). Previously, atmospheric turbidity had been studied by Hulbert (1937) using a searchlight. The experiment was perfected by Thickstun (1954), Friedland *et al* (1956) and Horman (1961). Actually, the original idea of probing the environment with light beams dates back to the experiments of Tyndall (1869). The advent of the laser brought several advantages, namely large intensities, short pulses, narrow beams, narrow bandwidth, well defined polarization and a high degree of coherence.

Since 1963, the field has progressed rapidly. New systems have been developed to extend the observable parameters, the range, the resolution, the signal-to-noise ratio, etc. Several high-performance lidars are now in operation around the world (Hinkley 1976, Ansmann *et al* 1997).

A lidar system for the observation of the stratosphere and the mesosphere, owned by the Institute of Atmospheric Physics (IFA), has been operational at Frascati, Italy, from 1981 to 1996 (Adriani *et al* 1983, 1984, Gobbi *et al* 1984). It was based upon a large mosaic telescope, made up of 36 mirrors, with a receiving surface of about 5 m^2, and was hosted in a four-story tower (8 m focal length). Additionally, a smaller receiver was located in a container located nearby. The use of a second receiver allowed a wide dynamic range of the backscattered signal (seven orders of magnitude), permitting one to simultaneously detect the backscattered echoes from the layers between $\sim$12 and $\sim$ 90 km in altitude. Profiles of temperature and density in the mesosphere and the upper stratosphere were obtained (Adriani *et al* 1988, 1991). Moreover, the system also measured the aerosol profiles of the lower and middle stratosphere (Adriani *et al* 1984, Gobbi *et al* 1992). In particular, within the dataset the evolution of the two major stratospheric perturbations of this century is documented; namely the eruptions of El Chichon (Mexico, March 1982) and Mount Pinatubo (Philippines, June 1991).

In late 1997, the Institute moved to a new location (Traversi and Pierini 1991): this has raised the problem of the future of the old system. In the first instance, there would have been several difficulties in the transfer of such a large telescope. Secondly, the new site is located at a lower altitude, and closer to the urban area of Rome, where both a higher turbidity (due to pollution) and a higher night-time sky background level (due to the city lights and the nearby expressway) are expected. Last but not least, despite the fact that the telescope is one of the largest among those used for

§ Present address: Agenzia Spaziale Italiana, Viale Regina Margherita 202, 00198 Rome, Italy.
‖ Present address: Fondazione Ugo Bordoni, Viale Europa 190, 00144 Rome, Italy.

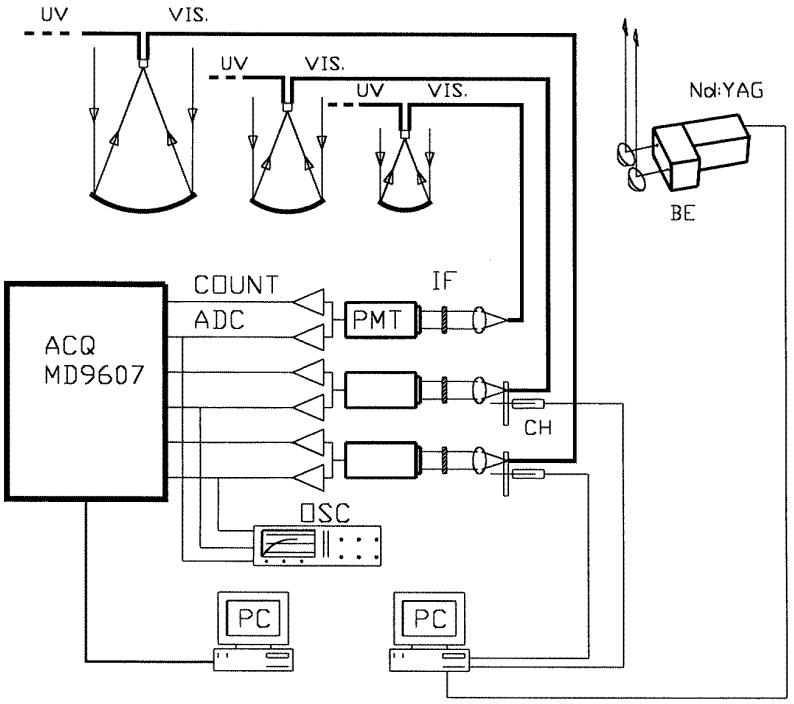

Figure 1. Schematic block diagram of '9-eyes'. Only the detectors for $\lambda = 532$ nm are depicted (the corresponding ones for $\lambda = 355$ nm are similar). The largest telescope drawn represents the nine-telescope array. Nd:YAG, laser; BE, beam expander; PMT, photomultiplier; IF, interference filter; CH, chopper; COUNT, photon count channel; ADC, analogue-to-digital channel.

lidar applications, it suffers from the fact that it was designed more than 25 years ago. As a matter of fact, it presents the following disadvantages:

(a) lack of flexibility;
(b) a complicated alignment procedure; and
(c) a large dimension of the focus, and thus the need to use a large acceptance angle (therefore increasing the background).

Instead, the option of a completely new system, occupying a smaller volume and designed with modern criteria, has been considered. This option combines the advantages of easier use, shorter assembly times and lower cost, with a similar performance. The new lidar will be assembled in two containers, to allow its transportability and its deployment at different locations. Small volume is combined with a large receiving surface through the use of a multiple-telescope light collector. The use of three different receiving channels also permits us to extend the profiles down to almost all of the troposphere. Moreover, vibrational Raman scattering channels provide the concentration of given gases (nitrogen, minor constituents).

2. System overview

The block diagram of '9-eyes' is shown in figure 1. The main specifications are listed in tables 1 and 2. The light pulses emitted at two wavelengths from the laser source are transmitted vertically upwards by using a mirror at 45°. The backscattered radiation is received by three separate collectors. Due to the wide dynamic range of the signal, between the planetary boundary layer (PBL) and the mesopause, it is impossible to use a single optical detector. The use of separate collectors allows us to divide the altitude range into smaller intervals, with smaller dynamic range. The three intervals partially overlap, to allow inter-normalization, and the re-constitution of a unique lidar profile extending from ∼0.3 to ∼90 km altitude. To each collector, there corresponds a different Newtonian telescope, or set of telescopes. Channel 1, which is used to detect the weak signal backscattered from very high up, is an array of nine telescopes (from which the name '9-eyes' derives). Each mirror focuses the incident light onto an optical system, where the visible and the ultraviolet components are split. These two components are carried separately to the detection system by optical fibres. The nine optical fibres corresponding to each of the two components for channel 1 are gathered together to the same endpoint.

At the other end of the optical fibre, a rotating wheel (chopper) filters out the light scattered by the lower layers, to avoid blinding the photomultipliers by too intense signals. Interference filters are used to reject light at non-emitted wavelengths, and thus to limit the contribution due to sky background. Photomultipliers (PMTs) are used as light

Table 1. Specifications of the transmitter.

Laser	Nd:YAG
Wavelengths	532 and 355 nm
Pulse energy	350 and 450 mJ
Repetition rate	10 Hz
Pulse duration (1064 nm)	6–8 ns
Pulse duration (532 nm and 355 nm)	5–7 ns
Beam divergence	∼0.15 mrad
Beam diameter	∼50 mm
Pointing stability	∼0.05 mrad

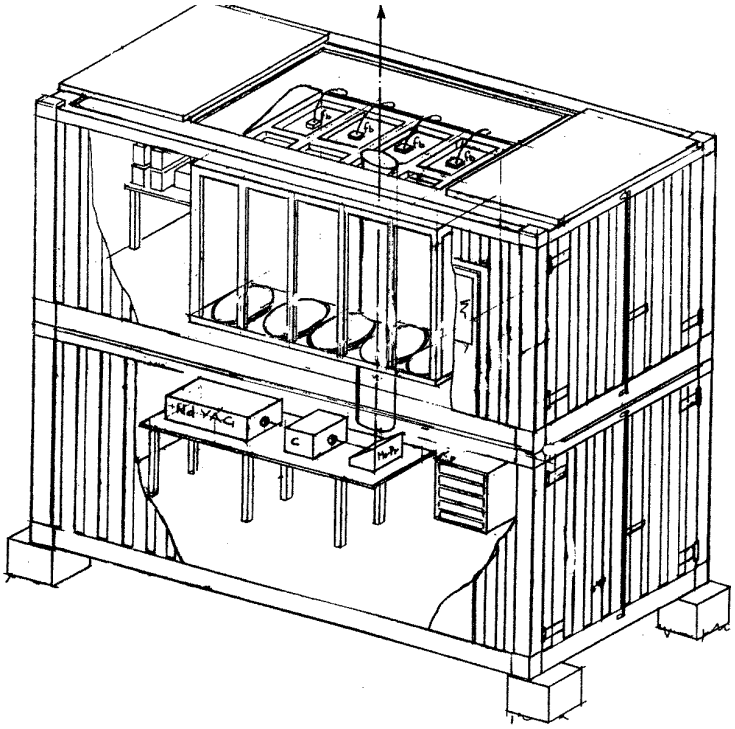

Figure 2. Configuration of the lidar '9-eyes': positioning of the containers.

Table 2. Specifications of the receiver.

Channel 1	9 Newtonian telescopes
Diameter	500 mm (each)
Focal length	1500 mm
Field of view	0.2–0.6 mrad (selectable)
Bandwidth	1 nm (532), 2 nm (355)
Sounding range	30–90 km
Complete overlap range	9 km (532 and 355)
Channel 2	Single Newtonian telescope
Diameter	300 mm
Focal length	900 mm
Field of view	0.3–1 mrad (selectable)
Bandwidth	1 nm (532), 2 nm (355)
Sounding range	2–45 km
Complete overlap range	1.8 km (532), 1.2 km (355)
Channel 3	Single Newtonian telescope
Diameter	150 mm
Focal length	450 mm
Field of view	0.6–2 mrad (selectable)
Bandwidth	1 nm (532), 2 nm (355)
Sounding range	0.3–6 km
Complete overlap range	350 m (532), 250 m (355)

detectors: their role is to convert the optical signal into electrical output. The signal is then amplified, and measured both by analogue-to-digital conversion and photon-counting techniques. A transient recorder acquires the signal variation as a function of time after the laser shot, averages on the desired number of laser pulses, and transfers the profiles to a personal computer, where they are stored. The range resolution ($\geqslant$75 m) is directly related to the signal sampling rate; the time resolution, related to the number of pulses on which averaging is performed, can be selected within a 0.1–4 h interval.

The system has to be transportable: it will therefore be assembled in standard containers for transportation by truck. Due to the large dimensions of the lidar, two containers will be necessary: one for the transmitter and the other one for the receiver. In order to achieve a better overlap between the emitted beam and the field-of-view of the receiver, a small horizontal distance between the laser and the mirrors is to be preferred. Therefore, the two containers are to be placed one of top of the other, with the receiver being on top, so that the beam will be emitted near the centre of the set of telescopes (see figure 2).

All components of the lidar have been purchased. Currently (June 1998), the most critical components and subsystems (PMTs, choppers and synchronization, beamsplitting devices) are being set up. The system is due to be ready for use in mid-1999.

3. The multiple-channel technique

Good photomultipliers used in lidar systems can maintain a linear response to signals spanning five orders of magnitude at most. When the intensity of the signal is too high (i.e. a signal coming from altitudes lower than the chosen range of observation), the detector is blinded and does not return to linear operation before a given delay. A chopper placed in front of each PMT, and synchronized with the laser pulse, is used to protect the detector from these large signals. A signal-induced noise with a time constant of typically several hundreds of microseconds would otherwise appear (Cairo *et al* 1996). The duration of this spurious signal is much longer than the decay of the backscattered signal from the atmosphere ($\sim 50\ \mu$s). The intensity of the signal is limited at

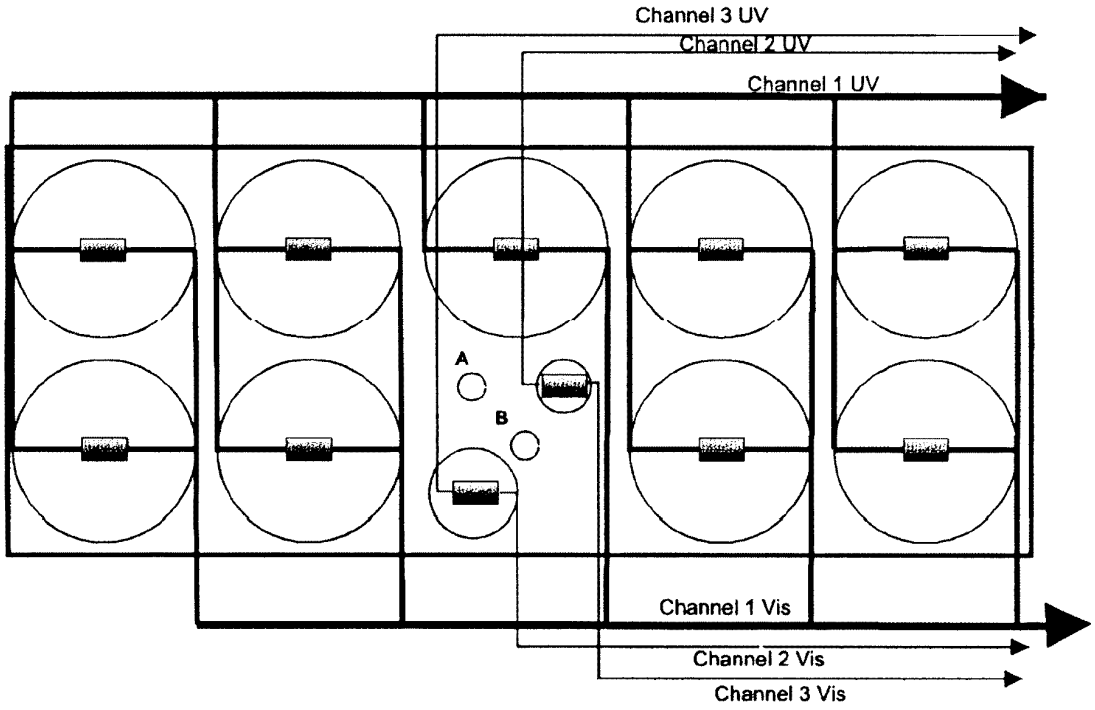

Figure 3. Mirror and optical fibre assembly, with optical separation of the visible and the UV wavelengths at the foci of the telescopes. The positions of the laser beams are also depicted ($A = 532$ nm, $B = 355$ nm).

the other end (low signal, i.e. high altitudes) by the signal-to-noise ratio (SNR). Trying to extend the observation range to lower altitudes thus has the effect of introducing an undesired systematic effect at the higher levels.

On the other hand, the signal backscattered by the atmosphere can span over several more orders of magnitude than can be measured with a single photomultiplier. It can be seen that about 13 orders of magnitude have to be considered, if one wants to obtain a lidar profile extending from ~ 0.3 to ~ 90 km. From these considerations, there follows the need to split the measuring range into three intervals, corresponding to three different channels. A wide overlapping altitude range has to be present between the intervals, to allow for inter-normalization, and thus the reconstruction of a unique lidar profile. The different channels, and the altitude intervals that correspond to them, are listed in table 2.

4. Transmitter

A Nd:YAG laser is used as the light source, with second and third harmonic generators. The emitted wavelengths are 532 and 355 nm. This choice follows from the high performance-to-cost ratio of this type of laser, since a relatively high emitted power can be achieved at wavelengths that are well adapted to both scattering by the atmosphere and efficiency of the detectors. Moreover, an excellent height resolution can be achieved, thanks to a pulse width as short as ~ 7 ns. The pulse repetition frequency (PRF) of the laser is 10 Hz, the beam divergence is around 0.5 mrad and the beam diameter is ~ 10 mm. Finally, a beam pointing stability comparable to the beam divergence is available with a good commercial laser. This allows one to use a small-enough receiver aperture.

The two transmitted wavelengths exit the laser separately, to allow for separate alignment. The two beams each pass into a beam expander, consisting of a divergent lens followed by a convergent lens. This brings the divergence down to ~ 100 μrad. As a consequence, the beam diameter increases by a factor of 5. Moreover, scattering from atmospheric inhomogeneities, and imperfections of the optics of the beam expander and of the mirror, may increase the output divergence. This additional divergence can be conservatively estimated as being smaller than 50 μrad, thus leading to an actual divergence of <150 μrad.

The light beams, emitted in the horizontal direction by the laser, are then transmitted vertically upwards by two mirrors oriented at 45° from the vertical. Precise computer-controlled motors control and fine-tune both the azimuth and zenith angles of the mirrors. An angular resolution of one order of magnitude smaller than the beam divergence is used to allow precise alignment.

5. Receiver

In the receiver, the following items are included:

(a) the collectors (telescopes);
(b) the optical devices selecting the signal to be measured (interference filters, choppers, etc);
(c) the photomultipliers;
(d) a dedicated electronic device for signal acquisition and fast averaging; and
(e) a personal computer that drives the electronics and saves the data on disk.

Figure 3 depicts the assembly of the telescopes. The collector of the principal optical channel (largest collector, i.e.

channel 1) is a set of nine telescopes, each of 50 cm diameter and 1.5 m focal length (giving an f-number of 3). The total receiving area is thus 1.75 m^2, and if a unique mirror with the same area had to be used, its diameter would be 1.5 m. The advantage of having several mirrors resides mainly in the smaller volume that can be achieved to obtain similar performance (e.g. with the same f-number, the single-mirror option would require a 4.5 m focal length). Moreover, this greatly reduces the cost of the mirrors. For the other two channels, single mirrors are used, of diameter 30 cm for channel 2 and 15 cm for channel 3. The f-number of 3 is kept, as for channel 1, and therefore the focal lengths are 90 and 45 cm, respectively.

At the focus of each telescope, a small optical system is placed, with the function of separating the visible wavelength (532 nm) from the ultraviolet one (355 nm). The beam is first collimated by a lens, and then separated into its two components by a dichroic beamsplitter, and the two beams are again focused onto optical fibres to transfer the light to the photodetection system. The output ends of the optical fibres arriving from the nine telescopes of channel 1 are grouped into the same bundle. This layout is depicted in figure 3.

Each of the 11 optical systems placed in the foci of the telescopes is positioned by computer-controlled X–Y–Z micrometric translators. The positioning accuracy (resolution and repeatability) is better than 5 μm, allowing the line of sight of each telescope to be varied in steps of ~ 3 μrad. The inter-alignment of the different telescopes is performed through the means of a horizontal mirror placed above each of them. The horizontality of the mirror can be controlled with an accuracy of ~ 20 μrad by two electronic inclinometers. The field of view of each telescope is controlled by a diaphragm included in the optical system.

Six different optical signals are thus carried to the subsequent analysing system by four single optical fibres and two bundles. They correspond to the three channels, each split into visible and ultraviolet signals. Each optical fibre is placed at the focus of a collimating lens. A rotating wheel (chopper) prevents the intense signals from reaching the PMT (except for channel 3). All choppers are synchronized with each other, and with the laser pulse, with separately tunable delays, with an accuracy of <10 μs. This technique, though it is not the simplest method to protect PMTs from strong signals, has the advantage over switching of dynode voltage that the photocathode is protected as well, and that electrical transients are suppressed. An interference filter matching the laser output wavelength sets the acceptance bandwidth.

After the wavelength separation, and the spectral and temporal filtering, each of the six beams reaches the window of the corresponding photodetector. The incident energy is spread over an area wide enough to reduce the risk of excessive intensities on the surface of the photocathode. The PMTs are THORN EMI 9954B for the 532 nm wavelength, and THORN EMI 9214QB for the 355 nm wavelength, and are cooled down to $-10\,^{\circ}$C. These models have been selected for the following characteristics: wide cathode area (diameter $>$ 40 mm), high quantum efficiency, short response time, high gain, wide dynamic range and small dark current. The corresponding dynode voltage divider networks have been designed to ensure the best linearity properties within the expected range of photon rates. The technical characteristics of the PMTs are summarized in table 3.

Table 3. Specifications of the THORN EMI photomultipliers used for '9-eyes'.

	532 nm	355 nm
Model	9954B	9214QB
Photocathode	RbCs	Bialkali
Effective cathode diameter	46 mm	46 mm
Quantum efficiency	0.14	0.25
Type of dynodes	BeCu	CsSb
Number of dynodes	12	12
Multiplier structure	linear focus	linear focus
Gain	4.5×10^6	8.3×10^6
Dark current ($-10\,^{\circ}$C)	$<$50 cps	$<$20 cps
Rise time	2 ns	2 ns
Transit time	41 ns	41 ns

Table 4. Specifications of the MD9607 transient recorder and multichannel counter.

Transient recorder	
Number of channels (separate inputs)	8
Input range	0–1 V or 0–5 V
Sampling frequency	5–20 MHz
Number of bits of ADC	12 bits
Number of bits of average register	16 bits
Multichannel counter	
Number of channels (separate inputs)	8
Discriminator threshold	40–1000 mV
Discriminator dead time	4 ns
Bin duration	0.5–500 μs
Number of bits of counter	16 bits
Number of bits of average register	32 bits

The output of the PMTs is analysed both in the photon-counting mode and by analogue-to-digital conversion. In the first case, the single photoelectron pulses that exceed a voltage threshold are turned into logical pulses by a discriminator. A multichannel counter records the number of photoelectrons for a set of time bins, the duration of each bin being selected for the desired vertical resolution. In the analogue-to-digital technique, the signal is first amplified, and then sampled at given intervals by a transient recorder. In both cases, signal acquisition is synchronized with the laser emission. A dedicated device, containing the discriminators, the multichannel counters, and the transient recorders, has been designed for these tasks. Its specifications are summarized in table 4. The device also performs fast averaging on a selected number of successive laser pulses, to improve the SNR. A personal computer is used to both drive the dedicated device and record the lidar profiles.

The project, in the final configuration, includes the detection of two Raman scattered signals, to measure the concentration of nitrogen and water vapour. This implies further wavelength separations after the output of two of the optical fibres, and additional detection channels (see figure 4).

The system design is based on the concept of flexibility. Changing the connections of the optical fibres allows

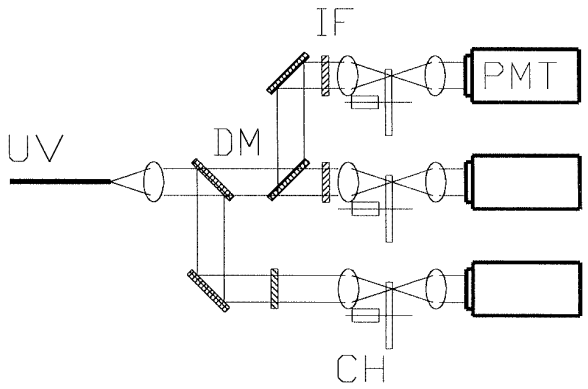

Figure 4. Raman wavelength separation in the final configuration of the lidar (UV only): the three PMTs are for elastic backscatter, N_2 and H_2O. The Raman capability can be installed on channel 1 (nine-telescope array) and channel 2 (intermediate telescope). DM, dichroic mirror; IF, interference filter; PMT, photomultiplier; CH, chopper. No choppers will be installed for the N_2 and H_2O signals on channel 2 (signal from the PBL).

different observation geometries. Moreover, by moving the field diaphragms out of axis on the mirror focal planes, the field of view of the individual telescopes can be tilted independently with high accuracy. Thanks to the computer-controlled micropositioners, the inclination of the field of view can be determined and reproduced to within a few μrad. By giving different tilts to the telescopes, multiple scattering from different atmospheric parts neighbouring the emitted beam can be studied. Quantification of multiple scattering is an important issue, for instance, for the analysis of space-borne lidar signals.

6. Observable quantities

'9-eyes' is a multipurpose system, designed for the simultaneous observation of different atmospheric parameters of the troposphere, the stratosphere and the mesosphere. The variables that can be measured are listed below.

(a) Vertical profiles of backscattering and extinction coefficients of the aerosols in the planetary boundary layer, in the free troposphere and in the lower stratosphere. The signal inversion method can be found in the papers by Fernald (1984), Klett (1985), Di Girolamo *et al* (1994) and Marenco *et al* (1997).

(b) Density and temperature profiles of the part of the middle atmosphere that is devoid of aerosols ($z > 30$ km). The method to deduce the density and temperature from the backscattered signal has been described by Hauchecorne and Chanin (1980) and by Jenkins *et al* (1987).

(c) Vibrational Raman technique (N_2): temperature profile in the presence of aerosols (troposphere and lower stratosphere). This is an extension of the Rayleigh technique used for $z > 30$ km (Keckhut *et al* 1990).

(d) Vibrational Raman technique (H_2O): vertical distribution of water vapour (Melfi 1972, Vaughan *et al* 1988).

(e) Properties of clouds: geometrical (height, depth); optical (optical thickness of thin clouds); statistical.

(f) Effects of multiple scattering in lidars.

Note that density and temperature measurements require only one wavelength (the second one is redundant). The same has to be said for simple aerosol backscattering and extinction coefficient retrieval, whilst aerosol particle size measurements require a minimum of three wavelengths. This might well be a future extension, obtainable by adding a receiver for the fundamental laser wavelength (1064 nm). The main reason for using two wavelengths in the basic configuration is that the visible is better for aerosol measurements (smaller extinction), whilst the ultraviolet is better for Raman signals (larger cross section).

7. Conclusion

'9-eyes' incorporates the latest technological developments in optical design, laser sources, detection electronics and data handling. The individual features are based on proven concepts, but their collection into a single transportable system is the innovative characteristic of the project.

Acknowledgments

The authors would like to thank Dr Alberto Bombonati and Area di Ricerca di Roma-Tor Vergata for financial, technical and administrative support for this project.

References

Ansmann A, Neuber R, Rairoux P and Wandinger U 1997 *Advances in Atmospheric Remote Sensing with Lidar* (Berlin: Springer)

Adriani A, Congeduti F, Fiocco G and Gobbi G P 1983 One year lidar observations of the stratospheric aerosol at Frascati, March 1982–March 1983 *Geophys. Res. Lett.* **10** 1005–8

Adriani A, Congeduti F, Gobbi G P, Ligi R and Fiocco G 1984 The El Chichon aerosol cloud observed by lidar in Frascati, March 1982–April 1984: backscattering and extinction *IRS 84: Current Problems in Atmospheric Radiation* ed G Fiocco (Hampton, VA: Deepak) pp 103–6

Adriani A, Di Donfrancesco G, Viterbini M, Gobbi G P and Congeduti F 1988 Lidar measurements of stratospheric and mesospheric density: preliminary results *Progress in Atmospheric Physics* ed R Rodrigo (Dordrecht: Reidel) pp 47–56

Adriani A, Gobbi G P, Congeduti F and Di Donfrancesco G 1991 Lidar observations of stratospheric and mesospheric temperature: November 1988–November 1989 *Ann. Geophys.* **9** 252–8

Cairo F, Congeduti F, Poli M, Centurioni S and Di Donfrancesco G 1996 A survey of the signal-induced noise in photomultiplier detection of wide dynamics luminous signals *Rev. Sci. Instrum.* **67** 3274–80

Di Girolamo P, Cacciani M, Di Sarra A, Fiocco G and Fuà D 1994 Lidar observations of the Pinatubo aerosol layer at Thule, Greenland *Geophys. Res. Lett.* **21** 1295–8

Fernald G F 1984 Analysis of atmospheric lidar observations: some comments *Appl. Opt.* **23** 652–3

Fiocco G and Smullin L D 1963 *Nature* **199** 1275–76

Friedland S S, Katzenstein J and Zatzick M R 1956 *J. Geophys. Res.* **61** 415–34

Gobbi G P, Ligi R, Adriani A, Fiocco G and Congeduti F 1984 Two-wavelength lidar observations of stratosphere and inference on the size distribution of the El Chichon aerosols *IRS 84: Current Problems in Atmospheric Radiation* ed G Fiocco (Hampton, VA: Deepak) pp 115–8

Gobbi G P, Congeduti F and Adriani A 1992 Early stratospheric effects of the Pinatubo eruption *Geophys. Res. Lett.* **19** 997–1000

Hauchecorne A and Chanin M-L 1980 Density and temperature profiles obtained by lidar between 35 and 70 km *Geophys. Res. Lett.* **7** 565–8

Hinkley E D 1976 *Laser Monitoring of the Atmosphere* (Berlin: Springer)

Horman M H 1961 *J. Opt. Soc. Am.* **51** 681–91

Hulbert E O 1937 *J. Opt. Soc. Am.* **27** 377–82

Jenkins D B, Wareing D P, Thomas L and Vaughan G 1987 Upper atmospheric temperatures derived from lidar observations at Aberystwyth *J. Atmos. Terrest. Phys.* **49** 287–98

Keckhut P, Chanin M L and Hauchecorne A 1990 Stratosphere temperature measurement using Raman lidar *Appl. Opt.* **29** 5182–6

Klett J D 1985 Lidar inversion with variable backscatter/extinction ratios *Appl. Opt.* **24** 1638–43

Ligda M G H 1963 *Proc. 1st Conf. on Laser Technol. (San Diego, CA)* (US Navy ONR) pp 63–72

Marenco F, Santacesaria V, Bais A F, Balis D, di Sarra A, Papayannis A and Zerefos C 1997 Optical properties of tropospheric aerosols determined by lidar and spectrophotometric measurements (PAUR campaign) *Appl. Opt.* **36** 6875–86

Melfi S H 1972 Remote measurements of the atmosphere using Raman scattering *Appl. Opt.* **11** 1605–10

Thickstun W R 1954 *Weatherwise* **7** 96–100

Traversi F and Pierini G 1991 Area di Ricerca Roma Tor Vergata

Tyndall J 1869 *Phil Mag.* **37** 384–94

Vaughan G, Wareing D P, Thomas L and Mitev V 1988 Humidity measurements in the free troposphere using Raman backscatter *Q. J. R. Meteorol. Soc.* **114** 1471–84